Supplementary information for

Precise graphene cutting by catalyst at the tip of a probe under electron beam

Alexander S. Sinitsa[a, b1], Yulia G. Polynskaya[b], Irina V. Lebedeva[c,d,e],

Andrey A. Knizhnik[b] and Andrey M. Popov[f]

[a] National Research Centre "Kurchatov Institute", Kurchatov Square 1, Moscow 123182, Russia.

[b] Kintech Lab Ltd., 3rd Khoroshevskaya Street 12, Moscow 123298, Russia.

[c] CIC nanoGUNE BRTA, Avenida de Tolosa 76, San Sebastian 20018, Spain.

[d] Catalan Institute of Nanoscience and Nanotechnology – ICN2, CSIC and BIST, Campus UAB, Bellaterra 08193, Spain

[e] Simune Atomistics, Avenida de Tolosa 76, San Sebastian 20018, Spain

[f] Institute for Spectroscopy of Russian Academy of Sciences, Fizicheskaya Street 5, Troitsk, Moscow 108840, Russia.

Contents

[1] Corresponding author. Tel. +7-903-668-9915 E-mail: alexsinitsa91@gmail.com (Alexander Sinitsa)

Structure evolution and time dependences of structural characteristics during graphene cutting: an example of the simulation run for cutting in the zigzag direction

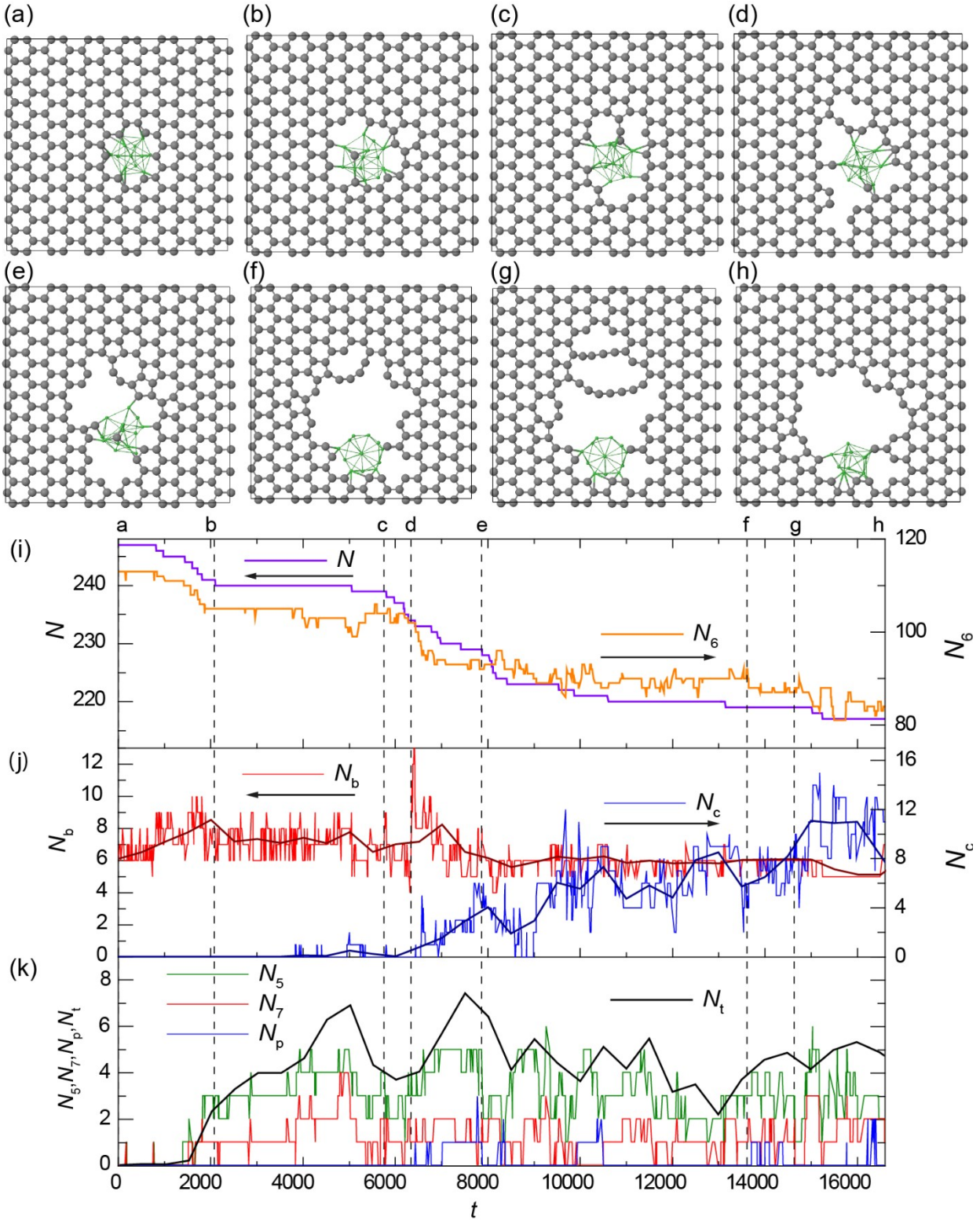

Figure S1. (a–j) Simulated structure evolution during graphene cutting in the armchair direction by a nickel tip under irradiation by electrons with a kinetic energy of 80 keV and a flux of $4 \cdot 10^6$ electrons/(s·nm^2) in HRTEM: (a) 0 s, (b) 2078 s, (c) 5752 s, (d) 6340 s, (e) 7870 s, (f) 13614 s (g) 14635 s and (h) 16692 s. (i-k) Calculated (i) total number of carbon atoms, N, in the considered structure (violet line, left axis), number of hexagons, N_6 (orange line, right axis), (j) instantaneous and average number of two-coordinate atoms in chains, N_c (thin and thick blue line, respectively,

right axis), instantaneous and average number of carbon atoms bonded to the nickel tip, N_b (thin and thick red line, respectively, left axis), (k) numbers of pentagons, heptagons and other polygons, N_5, N_7 and N_p respectively (green, red and blue lines, respectively) and average total number of polygons which are not hexagons, $N_t = N_5 + N_7 + N_p$ (thick black line), as functions of time, t (in s). Averaging is performed over 500 s. The moments of time corresponding to structures (a–h) are shown by vertical dashed lines.

Final structures obtained at the end of MD simulation runs of graphene cutting

Structures of the cuts obtained at the end of all performed simulation runs for the armchair and zigzag cutting directions are shown in Fig. S2 and S3, respectively. Structure evolution in the simulation runs corresponding to the cuts shown in Fig. S2a and Fig. S3a is shown in detail in Fig. 2 and Fig. S1, respectively.

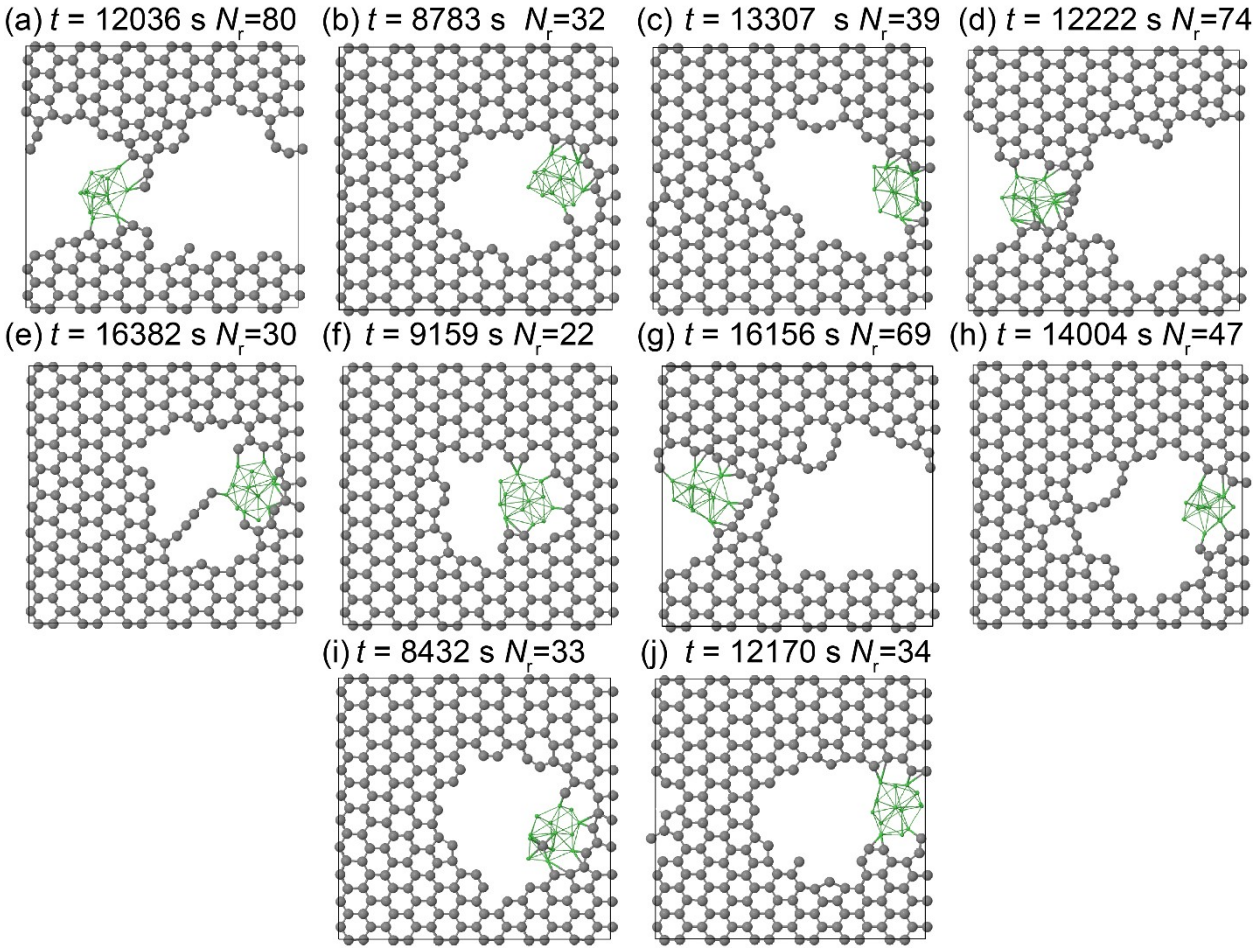

Figure S2. (a)-(j) Calculated structures of the cuts obtained at the end of all performed simulation runs of graphene cutting in the armchair direction by a nickel tip under irradiation by electrons with a kinetic energy of 80 keV and a flux of $4 \cdot 10^6$ electrons/(s·nm^2) in HRTEM. The time moment, t (in s), corresponding to the end of the performed simulation run and the number of carbon atoms removed, N_r, are indicated.

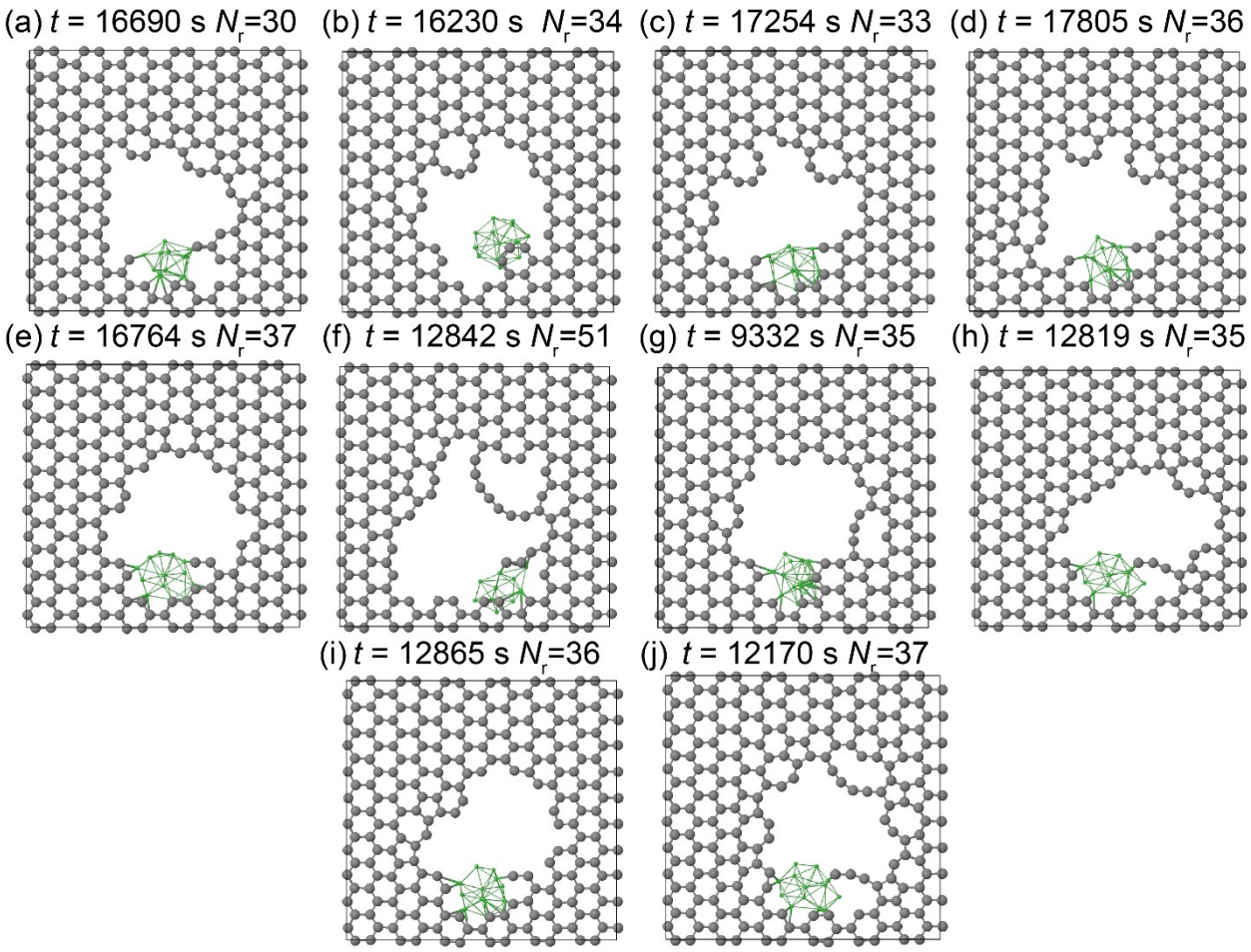

Figure S3. (a)-(j) Calculated structures of the cuts obtained at the end of all performed simulation runs of graphene cutting in the zigzag direction by a nickel tip under irradiation by electrons with a kinetic energy of 80 keV and a flux of $4 \cdot 10^6$ electrons/(s·nm^2) in HRTEM. The time moment, t (in s), corresponding to the end of the performed simulation run and the number of carbon atoms removed, N_r, are indicated.

An example of structure evolution during the tip detachment from graphene after complete cutting

The tip detachment process was considered both under electron irradiation in HRTEM and without electron irradiation. An example of the structure evolution during the tip detachment from the graphene layer under electron irradiation in HRTEM is shown in Fig. S4a-d. An example of the structure evolution during the tip detachment from the graphene layer without electron irradiation for the detachment time τ_{up} = 1000 ps and temperature T_{up} = 1800 K is shown in Fig. S4e-h.

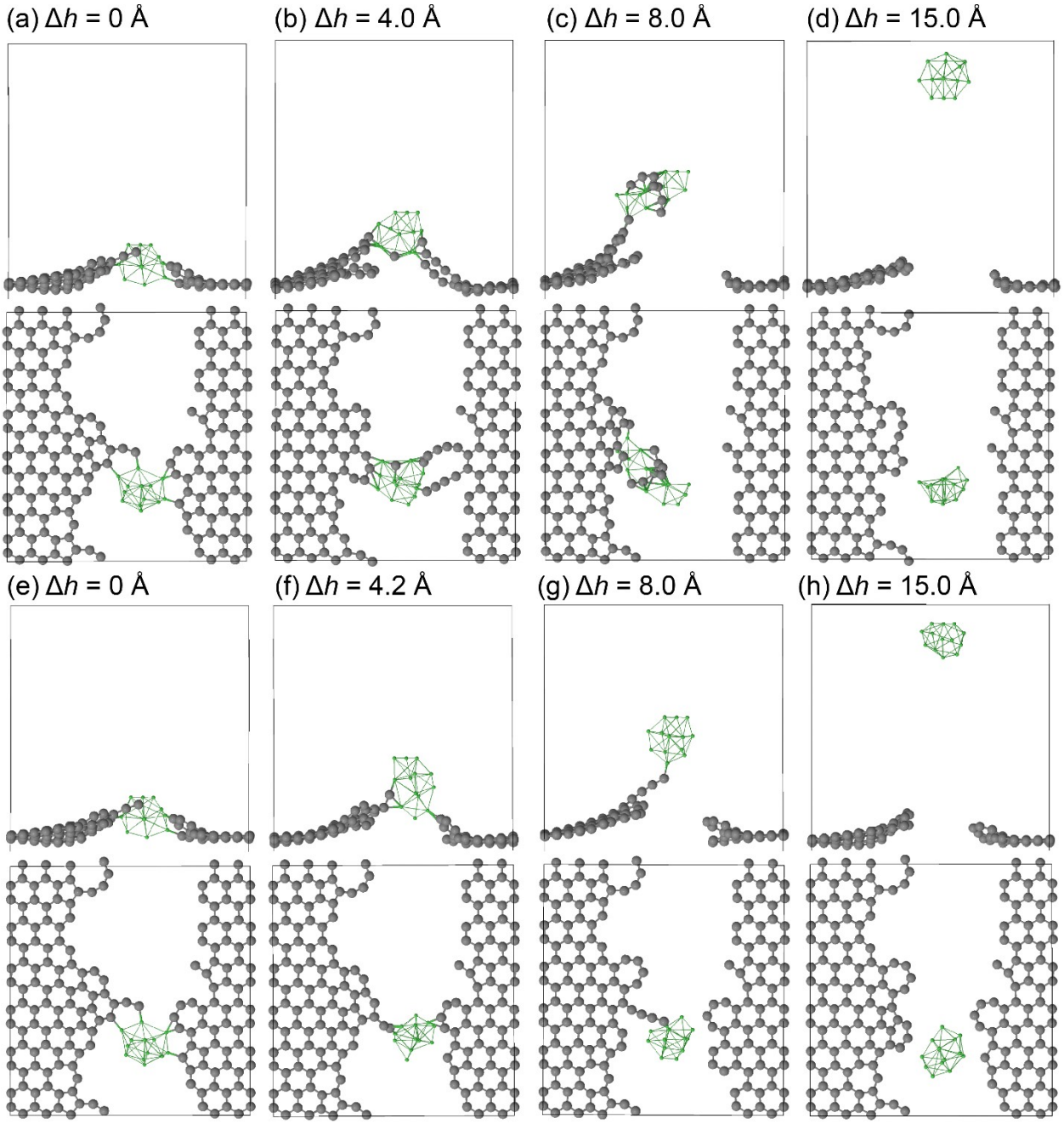

Figure S4. Simulated evolution of the graphene cut structure shown in Fig. S2a during the tip detachment (side view and top view rotated by 90 degrees for convenience) for detachment under electron irradiation in HRTEM (a)-(d) and without electron irradiation (e)-(h). The displacement, Δh, of the tip in the vertical direction away from the graphene plane relative the position during the cutting is indicated.

Description of video files

Video files “VID_GRCUT_AC.avi” and “VID_GRCUT_ZZ.avi” show examples of structure evolution observed in molecular dynamics simulations during graphene cutting in the armchair and zigzag directions, respectively. Video file “VID_GRCUT_AC.avi” corresponds to the simulation run shown in Figure 2, video file “VID_GRCUT_ZZ.avi” corresponds to the simulation run shown in Figure S1. For convenience, in the both videos, the viewpoint was shifted so that the cluster is positioned at the boundary of the simulation cell. Cutting occurs by simultaneous action of the nickel tip and irradiation by electrons with a kinetic energy of 80 keV and a flux of $4 \cdot 10^6$ electrons/(s·nm^2) in HRTEM. In these video files, carbon and hydrogen atoms are colored in grey and green, respectively. The total time in HRTEM (converted from the MD simulation time), current number of carbon atoms in the simulation cell, number of removed carbon atoms and number of nickel atoms in the simulation cell are given below the simulation cell.

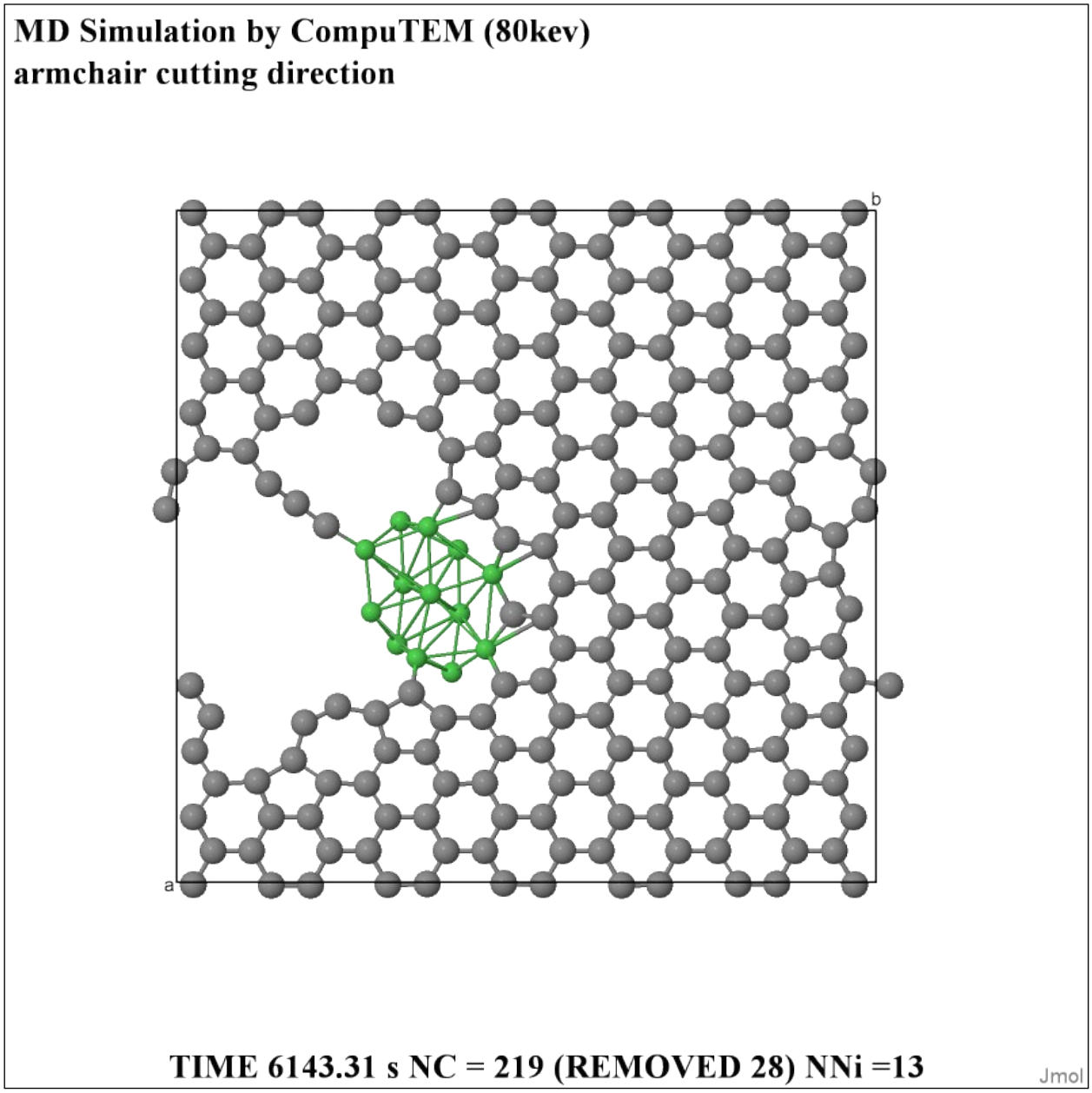

Nickel-carbon potential

The same as in the original Brenner potential (REBO-1990),[S1] the energy of the system in the reactive bond-order Ni-C potential (REBO-NiC-2012 from Ref. S2 and REBO-NiC-2014 from Ref. S3) is represented as

$$E_{\mathrm{b}} = \sum_{i} \sum_{j(>i)} E_{ij} \,, \tag{S1}$$

where the energy E_{ij} of the bond between atoms i and j separated by the distance r_{ij} is given by the sum of repulsive and attractive terms

$$E_{ij} = V_{\mathrm{R}}(r_{ij}) - \overline{b}_{ij} V_{\mathrm{A}}(r_{ij}) \,. \tag{S2}$$

The repulsive interaction is determined by the two-body function

$$V_{\mathrm{R}}(r_{ij}) = f_{ij}(r_{ij}) A_{ij} \exp\left(-\lambda_{1,ij} r_{ij}\right), \tag{S3}$$

where the cut-off function $f_{ij}(r)$ has the form

$$f_{ij}(r) = \begin{cases} 1, & r < R_{ij}^{(1)} \\ \dfrac{1}{2}\left[1 + cos\left[\dfrac{\pi(r - R_{ij}^{(1)})}{(R_{ij}^{(2)} - R_{ij}^{(1)})}\right]\right], & R_{ij}^{(1)} \le r \le R_{ij}^{(2)} \\ 0, & r > R_{ij}^{(2)} \end{cases} \tag{S4}$$

The attractive interaction is described by the two-body function

$$V_{A}(r_{ij}) = f_{ij}(r_{ij}) B_{ij} \exp\left(-\lambda_{2,ij} r_{ij}\right) \tag{S5}$$

multiplied by the function $\overline{b}_{ij}$ which describes the dependence of the interaction energy on the local coordination. The empirical bond order function $\overline{b}_{ij}$ is given by the sum of the average of the bond-order terms b_{ij} and b_{ji} corresponding to each atom in the bond and additional correction function F_{ij}, which is used to account for conjugated versus non-conjugated bonding and to distinguish radicals,

$$\overline{b}_{ij} = \left(b_{ij} + b_{ji}\right)/2 + F_{ij}\left(N_{ij}^{\mathrm{C}}, N_{ji}^{\mathrm{C}}, N_{ij}^{\mathrm{conj}}, N_{i}^{\mathrm{M}}, N_{j}^{\mathrm{M}}\right)/2 \,, \tag{S6}$$

where N_{ij}^{C} is the number of carbon atoms bonded to atom *i*, N_{i}^{M} is the number of metal atoms bonded to atom *i* and N_{ij}^{conj} is used to determine whether the bond between atoms *i* and *j* is a part of a conjugated system. The function F_{ij} is non-zero only for bonds between two carbon atoms.

The bond order function b_{ij} for each atom in the bond is determined by

$$b_{ij} = \left[1 + \sum_{k(\neq i,j)} G_{ijk}(\theta_{ijk}) f_{ik}(r_{ik}) \exp\left[\alpha_{ijk}\left(\left(r_{ij} - R_{ij}^{(\mathrm{e})}\right) - \left(r_{ik} - R_{ik}^{(\mathrm{e})}\right)\right)\right] + H_{ij}\left(N_{i}^{\mathrm{M}}, N_{j}^{\mathrm{C}}\right)\right]^{-\delta}, \tag{S7}$$

where $R_{ij}^{(\mathrm{e})}$ is the equilibrium distance between atoms *i* and *j*, θ_{ijk} is the angle between the bonds between atoms *i* and *j* and atoms *i* and *k* and δ is taken equal to 0.5 for all atoms. The function *H* in this expression is used to improve the description of low-coordinated nickel atoms. The function $G_{ijk}(\theta)$ is taken in the form

$$G_{ijk}(\theta) = a_{ijk}\left[1 + \frac{c_{ijk}^2}{d_{ijk}^2} - \frac{c_{ijk}^2}{d_{ijk}^2 + \left(1 + cos\,\theta\right)^2}\right]. \tag{S8}$$

As opposed to the original Brenner potential[S1], we assume that the parameters of the function $G_{ijk}(\theta)$, a_{ijk}, c_{ijk} and d_{ijk}, depend on types of all three atoms *i* , *j* and *k*.

The numbers N_{ij}^{C} and N_{ij}^{conj} are found as

$$N_{ij}^{\mathrm{C}} = \sum_{\mathrm{C}\,k(\neq j)} f_{ik}(r_{ik}), \tag{S9}$$

$$N_{ij}^{\mathrm{conj}} = 1 + \sum_{\mathrm{C}\,k(\neq i,j)} f_{ik}(r_{ik}) F_0(N_{ki}^{\mathrm{C}}) + \sum_{\mathrm{C}\,l(\neq i,j)} f_{jl}(r_{jl}) F_0(N_{lj}^{\mathrm{C}}), \tag{S10}$$

where

$$F_0(x) = \begin{cases} 1, & x \le 2 \\ \left[1 + \cos\left(\pi(x-2)\right)\right]/2, & 2 < x < 3 \\ 0, & x \ge 3 \end{cases} \tag{S11}$$

The parameters for nickel-nickel interactions were fitted to the experimental data on the lattice constant, cohesive energy, vacancy formation energy and elastic behavior for fcc Ni.[S2] It properly describes the relative stability of bulk Ni phases and Ni surfaces as well as the energies of formation of Ni adatoms and addimers on the (111) surface.[S2] In the present version of the Ni-C potential REBO-NiC-2023, we have modified the *F* function in eq. (6) so that it goes to zero in the case when the considered pair of carbon atoms has bonds with metal atoms. In this way we achieve two goals: (1) the description of binding of graphene edges with nickel surfaces is considerably improved and (2) changes in the *F* function for purely carbon systems do not affect energetics of carbon structures on the nickel surface, i.e. such corrections do not require further reconsideration of the parameters for carbon-nickel interactions. Additionally, in REBO-NiC-2023 we take into account corrections introduced in the potential for pure carbon systems REBO-1990EVC from Refs. S4 and S5 related to the better description of graphene edge energies, formation energy of carbon chains and barrier for vacancy migration. For REBO-NiC-2023, we have also refitted the binding energies of carbon adatoms and small carbon structures on the Ni(111) surface to more accurate DFT results for the bigger 4x4 model cell.

The two-body part of REBO-NiC-2023 is the same as for REBO-NiC-2014 (Table S1). The difference is in the parameters α_{ijk} ,a_{ijk}, c_{ijk} and d_{ijk} for nickel-carbon interactions (Table S2). Furthermore, the function F has been changed according to REBO-1990EVC (Table S3). As mentioned above $F_{\mathrm{CC}}\left(N_{ij}^{\mathrm{C}}, N_{ji}^{\mathrm{C}}, N_{ij}^{\mathrm{conj}}, N_i^{\mathrm{M}}, N_j^{\mathrm{M}}\right) = F_{\mathrm{CC}}\left(N_{ij}^{\mathrm{C}}, N_{ji}^{\mathrm{C}}, N_{ij}^{\mathrm{conj}}\right)$ only for $N_i^{\mathrm{M}} = N_i^{\mathrm{M}} = 0$, i.e. only when none of carbon atoms *i* and *j* is bonded to metal atoms. In the opposite case, $F_{\mathrm{CC}} = 0$. The function H is now nonzero only for $H_{\mathrm{MC}}\left(N_i^{\mathrm{M}}, N_j^{\mathrm{C}}\right)$ and equals 2.7 for $N_i^{\mathrm{M}} \le 4$ and any N_i^{C}.

To get more accurate values of energies of adatoms and other species we have repeated the DFT calculations for the extended 4x4 model cell of the Ni (111) surface. The same model cell is then used for fitting the potential. The DFT calculations have been performed using VASP code[S6] with the Perdew-Wang exchange-correlation functional.[S7] The basis set consists of plane waves with the maximum kinetic energy of 400 eV. The interaction of valence electrons with atomic cores is described using ultrasoft nonlocal pseudopotentials.[S8] A second-order Methfessel–Paxton smearing[S9] with a width of 0.1 eV is applied. Integration over the Brillouin zone is carried out using the Monkhorst-Pack method[S10] with 7 x 7 x 1 k-point sampling. The four-layer metal slabs are separated by a 10 Å vacuum gap. The structures are geometrically optimized until the residual force acting on each atom becomes less than 0.01 eV/Å.

Table S1. Two-body parameters of the potential.

Parameters	C-C	C-Ni	Ni-Ni
A (eV)	2606	1866	1473
B (eV)	1397	184.6	61.24
λ_1 (Å^{-1})	3.2803	3.6768	3.2397
λ_2 (Å^{-1})	2.6888	1.8384	1.2608
$R^{(1)}$ (Å)	1.7	2.2	3.0
$R^{(2)}$ (Å)	2.0	2.5	3.3
$R^{(e)}$ (Å)	1.3900	1.6345	2.0839

Table S2. Three-body parameters of the revised potential (the parameters changed as compared to REBO-NiC-2014 versions are shown in bold).

Parameters	CCC	**CCNi**	**CNiC**	**CNiNi**	NiNiNi	NiNiC	**NiCNi**	**NiCC**
α (Å^{-1})	0	0	0	0	4.40	0	**3.40**	0
a	$2.08\cdot10^{-4}$	**0.102**	**0.600**	**$3.14\cdot10^{-3}$**	$9.28\cdot10^{-2}$	0	**$1.94\cdot10^{-4}$**	**$1.78\cdot10^{-5}$**
c	330	0	0	**5.56**	7756	0	**7414**	**240**
d	3.50	1.00	1.00	**0.377**	69.0	1.00	**7.68**	**1.00**

The results for the new and previous versions of the Ni-C potential in comparison with the DFT data on relative energies of carbon structures on the Ni (111) surface and in the Ni bulk are given in Table S4 (structures for a smaller model cell are shown in Figure 1 of Ref. 2). It is seen that in general, the new potential REBO-NiC-2023 describes the energetics of carbon structures interacting with nickel better, especially carbon interstitials, C_6 and graphene.

To check the binding energy between graphene edges and the Ni (111) surface for REBO-NiC-2014 and REBO-NiC-2023, a zigzag graphene nanoribbon of 7.3 Å width is placed vertically with respect to the surface, which corresponds to the energy favorable position of the graphene edge with respect to the surface. Two structures with the graphene nanoribbon close to the surface and far from the surface are geometrically optimized and the energy difference between them divided by the nanoribbon length is obtained. The binding energy for the zigzag graphene edge on the Ni (111) surface for REBO-NiC-2014 is found to be only –0.38 eV/Å. This is considerably smaller in magnitude than the values obtained by DFT calculations for zigzag carbon nanotubes of about –1 eV/ Å (Ref. S11). According to REBO-NiC-2023, the binding energy of zigzag graphene edges is –1.10 eV/ Å, close to the DFT data.

Table S3. Values of function $F_{CC}(i,j,k)$ for integer values of i,j and k (the parameters changed as compared to REBO-NiC-2014 are shown in bold). Between integer values of i,j and k, the function is interpolated by a cubic spline. All parameters not given are equal to zero, $F_{CC}(i,j,k>2)=F_{CC}(i,j,k)$.

	F_{CC}
(0,1,1), (1,0,1)	0.0996
(0,2,1), (2,0,1)	0.0427
(0,2,2), (2,0,2)	-0.0269
(0,3,1), (3,0,1)	-0.0904
(0,3,2), (3,0,2)	-0.0904
(1,1,1)	0.1264
(1,1,2)	**0.02514818**
(1,2,1), (2,1,1)	0.0120
(1,2,2), (2,1,2)	**-0.0380**
(1,3,1), (3,1,1)	-0.0903
(1,3,2), (3,1,2)	-0.0903
(2,2,1)	0.0605
(2,3,1), (3,2,1)	-0.0363
(2,3,2), (3,2,2)	**-0.0880**

Table S4. Energies (in eV/atom) of carbon adatoms at different sites of the Ni (111) surface, carbon atoms in C_6 and in graphene on the Ni (111) surface, and carbon interstitials at the O (octahedral) and T (tetrahedral) sites in the first and second subsurface layer relative to the energy of a carbon adatom at the hcp site of the Ni (111) surface and absolute adsorption energy of a carbon atom at this site calculated for the considered 4x4x4 model cell. The relative energies of carbon interstitials at the O (octahedral) and T (tetrahedral) sites in the bulk are also indicated. The energies are given for geometrically optimized structures.

Structure	DFT (present work)	DFT (previous works)	REBO-NiC-2014 (Ref. 3)	REBO-NiC-2023
C at hcp site (absolute adsorption energy)	–6.81	–6.68,[S12] –6.87,[S13] –6.88,[S14] –7.0,[S15] –7.25[S16]	–5.95	–6.23
C at fcc site	0.057	0.042,[S13] 0.05,[S12, S17, S18] 0.056,[S2] 0.07,[S16] 0.073[S14]	0.0141	0.0190
C at bridge site	0.30	0.33,[S13] 0.34,[S2] 0.37,[S16] 0.39,[S18] 0.4,[S15, S19, S20] 0.5[S17, S21]	0.441	0.298
C at top site	2.4	2.35,[S2] 2.40[S13]	2.19	2.30
C at (100) step site		–0.32,[S18] –0.96,[S12] –0.98,[S2] –1.00,[S17, S22] –1.01,[S23] –1.03[S24]	–0.812	–0.835
C_6 with atoms at bridge sites	–0.121	–0.33[S2]	–0.347	–0.121
C_6 with atoms at hcp/fcp sites	–0.095	–0.29[S2]	–0.245	–0.0950
graphene	–1.10	–1.10,[S22] –1.17,[S12] –1.30,[S17] –1.35,[S2, S23]	–1.42	–1.14
C at O site of 1st subsurface layer	–0.45	–0.34,[S17] –0.42,[S18] –0.47,[S2, S14, S25] –0.5,[S15] –0.54,[S20] –0.57[S12, S13]	–0.601	–0.470
C at O site of 2nd subsurface layer	–0.14	–0.13,[S20] –0.17,[S13] –0.2,[S15] –0.25[S13, S25]	–0.272	–0.0167
C at T site of 2nd subsurface layer	0.80	1.34[S13]	0.810	1.29
C at bulk O site		–0.02,[S17] –0.16,[S18] –0.18,[S2] –0.2,[S15] –0.25,[S14] –0.32[S12]	–0.142	0.133
C at bulk T site		1.49,[S2] 1.76[S18], 1.8[S17,S18]	0.986	1.55

References

[S1] Brenner, D. W. *Phys. Rev. B* 1990, **42**, 9458–9471.
[S2] I. V. Lebedeva, A. A. Knizhnik, A. M. Popov and B. V. Potapkin, *J. Phys. Chem. C,* 2012, **116**, 6572.
[S3] A. S. Sinitsa, I. V. Lebedeva, A. A. Knizhnik, A. M. Popov, S.T. Skowron and E. Bichoutskaia, *Dalton Trans.* 2014, **43**, 7499–7513.
[S4] A. S. Sinitsa, I. V. Lebedeva, A. M. Popov and A. A. Knizhnik, *Carbon*, 2018, **140**, 543–556.
[S5] A. S. Sinitsa, I. V. Lebedeva, A. M. Popov and A. A. Knizhnik, *Carbon* 2019, **146**, 841.
[S6] G. Kresse, J. Furthmüller, *Phys. Rev. B* 1996, **54**, 11169–11186.
[S7] J. P. Perdew, Y. Wang, *Phys. Rev. B* 1992, **45**, 13244–13249.
[S8] G. Kresse, J. Hafner*, J. Phys.: Condens. Matter* 1994, **6**, 8245–8257.
[S9] M. Methfessel, A. T. Paxton, *Phys. Rev. B* 1989, **40**, 3616–3621.
[S10] H. J. Monkhorst, J. D. Pack, *Phys. Rev. B* 1976, **13**, 5188–5192.
[S11] F. Ding, P. Larsson, J. A. Larsson, R. Ahuja, H. Duan, A. Rosen, K. Bolton, *Nano Lett.* 2008, **8**, 463.
[S12] D. Cheng, G. Barcaro, J.-C. Charlier, M. Hou, A. J. Fortunelli, *Phys. Chem. C* 2011, **115**, 10537–10543.
[S13] Y.-A. Zhu, Y.-C. Dai, D. Chen, W.-K. Yuan, *Surf. Sci.* 2007, **601**, 1319–1325.
[S14] J. Xu and M. Saeys, *J. Catal.* 2006, **242**, 217–226
[S15] Y.-H. Shin, S. Hong, *Appl. Phys. Lett.* 2008, **92**, 043103.
[S16] Q.-M. Zhang, J. C. Wells, X. G. Gong, Z. Zhang, *Phys. Rev. B* 2004, **69**, 205413.
[S17] F. Abild-Pedersen, J. K. Nørskov, J. R. Rostrup-Nielsen, J. Sehested, S. Helveg, Phys. Rev. B 2006, **73**, 115419.
[S18] O. V. Yazyev, A. Pasquarello, *Phys. Status Solidi B* 2008, **245**, 2185–2188.
[S19] S. Hofmann, G. Csányi, A. C. Ferrari, M. C. Payne, J. Robertson, *Phys. Rev. Lett.* 2001, **95**, 036101.
[S20] I. V. Lebedeva, A. A. Knizhnik, A. V. Gavrikov, A. E. Baranov, B. V. Potapkin, S. J. Aceto, P.-A. Bui, C. M. Eastman, U. Grossner, D. J. Smith, T. J. Sommerer, *Carbon* 2011, **49**, 2508–2521.
[S21] S. Helveg, C. Lopez-Cartes, J. Sehested, P. L. Hansen, B. S. Clausen, J. R. Rostrup-Nielsen, F. Abild-Pedersen, J. K. Nørskov, *Nature* 2004, **427**, 426–429.
[S22] S. Saadi, F. Abild-Pedersen, S. Helveg, J. Sehested, B. Hinnemann, C. C. Appel, J. K. Nørskov, *J. Phys. Chem. C* 2010, **114**, 11221–11227.
[S23] H. S. Bengaard, J. K. Nørskov, J. Sehested, B. S. Clausen, L. P. Nielsen, A. M. Molenbroek, J. R. Rostrup-Nielsen*, J. Catal.* 2002, **209**, 365–384.
[S24] M.P. Andersson, F. Abild-Pedersen, *Surf. Sci.* 2007, **601**, 649–655.
[S25] J. Xu and M. Saeys, *J. Phys. Chem. C* 2008, **112**, 9679–9685.